ACS Chemical Neuroscience

Research Article

pubs.acs.org/chemneuro

The Isomeric Preference of an Atypical Dopamine Transporter Inhibitor Contributes to Its Selection of the Transporter Conformation

Ara M. Abramyan,[†] Sebastian Stolzenberg,[‡] Zheng Li,[§] Claus J. Loland,[∥] Frank Noé,[‡] and Lei Shi*[,†,§]

[†]Computational Chemistry and Molecular Biophysics Unit, Molecular Targets and Medications Discovery Branch, NIH/NIDA/IRP, Baltimore, Maryland 21224, United States

[‡]Computational Molecular Biology group, Institute for Mathematics, Freie Universität Berlin, Arnimallee 6, 14195 Berlin, Germany

[§]Department of Physiology and Biophysics, Weill Cornell Medical College of Cornell University, New York, New York 10065, United States

[∥]Molecular Neuropharmacology Group, Department of Neuroscience and Pharmacology, The Faculty of Health Sciences, The Panum Institute, University of Copenhagen, DK-2200 Copenhagen, Denmark

S *Supporting Information*

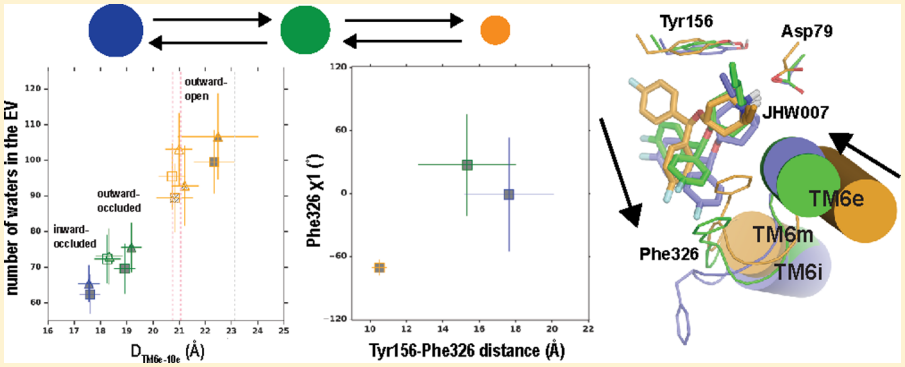

ABSTRACT: Cocaine, a widely abused psychostimulant, inhibits the dopamine transporter (DAT) by trapping the protein in an outward-open conformation, whereas atypical DAT inhibitors such as benztropine have low abuse liability and prefer less outward-open conformations. Here, we use a spectrum of computational modeling and simulation approaches to obtain the underlying molecular mechanism in atomistic detail. Interestingly, our quantum mechanical calculations and molecular dynamics (MD) simulations suggest that a benztropine derivative JHW007 prefers a different stereoisomeric conformation of tropane in binding to DAT compared to that of a cocaine derivative, CFT. To further investigate the different inhibition mechanisms of DAT, we carried out MD simulations in combination with Markov state modeling analysis of wild-type and Y156F DAT in the absence of any ligand or the presence of CFT or JHW007. Our results indicate that the Y156F mutation and CFT shift the conformational equilibrium toward an outward-open conformation, whereas JHW007 prefers an inward-occluded conformation. Our findings reveal the mechanistic details of DAT inhibition by JHW007 at the atomistic level, which provide clues for rational design of atypical inhibitors.

KEYWORDS: *Cocaine, dopamine transporter, atypical inhibitor, molecular dynamics, Markov state model analysis*

INTRODUCTION

The dopamine transporter (DAT) terminates neurotransmission of dopamine by reuptake of the neurotransmitter from the synaptic cleft back to the dopaminergic neurons.[1] Dysfunction of dopaminergic signaling is associated with a number of diseases including schizophrenia, Parkinson's disease, bipolar disorder, depression, and attention deficit hyperactivity disorder.[2−4] In addition, DAT is the primary target for several abused psychostimulants, including cocaine and amphetamines.[5−7] Cocaine, a highly addictive drug, competitively inhibits the function of DAT, which leads to dopamine accumulation in the synaptic cleft. DAT inhibition is known to be the driving force for the locomotor stimulant and reinforcing properties of cocaine in humans.[8] It had been hypothesized that all DAT inhibitors would produce behavioral effects identical to those of cocaine, i.e., increased rewarding effects, increased locomotor activity, and high abuse liability.[9−11] However, a large number of studies over the past 10−15 years have shown that several classes of DAT inhibitors, such as benztropine (BZT), modafinil, and some of their analogues have reduced

Received: March 10, 2017
Accepted: April 25, 2017
Published: April 25, 2017

DOI: 10.1021/acschemneuro.7b00094
ACS Chem. Neurosci. 2017, 8, 1735−1746

rewarding effects, and decreased abuse and addiction liability.[12−14] These compounds are termed "atypical inhibitors".[13] Moreover, one of the BZT derivatives, JHW007, was shown to antagonize the behavioral effects of cocaine and, thus, it is considered as a potential lead for treating psychostimulant abuse.[15,16] However, an atomistic understanding of the structural basis for differential effects of JHW007 and other atypical inhibitors, which would inform future drug design, remains unclear.

DAT and other members of the neurotransmitter:sodium symporter (NSS) family accomplish the thermodynamically unfavorable transport of substrates across the cell membrane by undergoing conformational transitions that are driven by the transmembrane Na^+ gradient.[7] Furthermore, mammalian NSS proteins are characterized by cotransport of Cl^-.[7,17] During the transport cycle, these transitions follow the alternating access mechanism,[18] in which the protein toggles between outward-facing (including both outward-open and outward-occluded) and inward-facing (including both inward-open and inward-occluded) conformations. The equilibrium between these conformations can be shifted by mutations and/or ligand binding.[19,20] For a bacterial homologue of NSS, leucine transporter (LeuT), the outward-open, outward-occluded, and inward-open conformations have been captured by X-ray crystallography.[21,22] Recent crystal structures of *Drosophila melanogaster* DAT (which shares more than 50% sequence identity with human DAT (hDAT), as opposed to ∼20% between LeuT and hDAT) have been solved in the presence of various substrate and inhibitors.[23,24] With the exception of the 3,4-dichlorophenylamine (DCP)-bound structure in a "partially" outward-occluded conformation, all of these structures were crystallized in outward-open conformations.

Based on the crystal structures of LeuT and dDAT, computational modeling and simulations have shed light on molecular mechanisms of the ligand binding as well as conformational dynamics in hDAT.[25−32] In particular, previous molecular modeling based on the LeuT structure in combination with a mutagenesis study predicted that cocaine and its high affinity analog 2β-carbomethoxy-3β-(4-fluorophenyl)tropane (CFT) disrupted an intramolecular interaction between Tyr156 and Asp79 in the central binding (S1) site of hDAT.[33] Removal of this interaction by Y156F mutation did not affect the binding affinity of cocaine or CFT to DAT, whereas binding of the atypical DAT inhibitor, JHW007 was reduced.[33] The recent crystal structures of dDAT bound to cocaine or CFT, however, show that the hydrogen bond between Tyr156 and Asp79 is intact and argue that the destabilization of this interaction is not directly involved in promoting the binding of cocaine or CFT.[24] Interestingly, the crystal structure of the Y108F mutant in LeuT (equivalent to Y156F in hDAT) has been found to be in the outward-open conformation (PDB ID 3TT1[21]).

Identification and characterization of the specific conformations that are differentially stabilized by the atypical and typical inhibitors are crucial in understanding their mechanisms of actions. Several studies have investigated the relationship between the conformational changes in DAT and the atypical effects of BZT and its derivatives.[34,35] In particular, the Y335A DAT mutation, which has been shown to steer DAT toward the inward-open conformation,[36] was found to affect the binding of atypical inhibitors much less than cocaine-like inhibitors.[34,37] Another mutagenesis and docking study demonstrated BZT and JHW007 interacted with Ala479 and Ala480 in transmembrane segment 10 (TM10), whereas this interaction was absent for CFT.[38] Taken together, previous studies on typical and atypical DAT inhibitors showed that the ligand-induced conformational changes in DAT as well as the binding mode of ligands have profound effects on the behavioral response produced by inhibitors. However, these studies have been limited by the absence of high-resolution DAT structures and the fact that modeling studies have been limited to docking or relatively short molecular dynamics (MD) simulations. Hence, the molecular details of the inhibition mechanism by atypical inhibitors and importantly, the protein's conformational changes induced by these inhibitors remain unclear.

Here we carry out more than 36 μs long MD simulations of six conditions, including WT and Y156F hDAT in the absence of any ligand (*apo*), or the presence of either JHW007 or CFT (Table 1), which are guided and analyzed with Markov state models (MSM). MSMs provide an efficient approach by stitching together a set of relatively short MD simulations into a single statistical model to describe the dynamics of proteins in terms of transitions between conformational states,[39,40] and have been successfully applied in revealing protein−ligand binding modes and protein conformational transitions.[41−45] Moreover, a recent MD simulation study in combination with MSM analysis identified the role of N-terminus in the mechanisms of Na^+ release from hDAT as the transporter transitions from outward-facing to inward-facing conformational states.[46] Our results demonstrate that JHW007 stabilizes hDAT in a conformation in between outward-occluded and inward-open conformations, whereas CFT and the Y156F mutation shift the conformational equilibrium toward an outward-open conformation.

Table 1. Simulated Conditions and Simulation Lengths

construct	ligand	no. of trajectories	trajectory lengths (μs)	aggregated lengths (μs)
WT	*apo*	12	9 × 0.3, 1 × 0.6, 2 × 0.9	5.10
	JHW007 (equatorial)	13	4 × 0.3, 1 × 0.42, 1 × 0.6, 4 × 0.9, 1 × 1.2, 1 × 1.2,[a] 1 × 0.72[a]	8.94
	JHW007 (axial)	6	2 × 0.6, 2 × 1.5, 2 × 0.9[a]	6.00
	CFT	3	1 × 0.6, 1 × 0.72, 1 × 1.2	2.52
Y156F	*apo*	9	6 × 0.3, 3 × 0.9	4.50
	JHW007	11	5 × 0.3, 1 × 0.6, 4 × 0.9, 1 × 1.2	6.90
	CFT	3	1 × 0.6, 2 × 0.9	2.40
total		**57**		**36.36**

[a]Simulations performed with the OPLS3 force field.

RESULTS

Overview of MD Simulations. We first carried out comparative simulations to identify the preferred isomer of JHW007, in terms of the axial versus equatorial form of the hydrogen attached to the nitrogen in the tropane ring (tNH), in binding to hDAT. We then initiated a set of simulations for six conditions, WT and Y156F hDAT in the absence of any ligand (*apo*), or the presence of either JHW007 or CFT, which are listed in Table 1. To adequately sample different hDAT conformational states and ligand binding modes, the initial

DOI: 10.1021/acschemneuro.7b00094
ACS Chem. Neurosci. 2017, 8, 1735−1746

simulations were followed by several rounds of additional simulations, in which we restarted trajectories from the under-sampled microstates according to the MSM analysis (see Methods). Overall, 57 full-atomistic MD simulation trajectories with aggregated simulation time of 36.36 μs (Table 1) were collected.

The Axial and Equatorial Isomers of JHW007 Differ in Their Stability and Binding to hDAT. Both CFT and JHW007 are tropane alkaloid derivatives and the tNH can adopt either an axial or an equatorial conformation (Figure 1A). Solution NMR studies have shown that the aryl

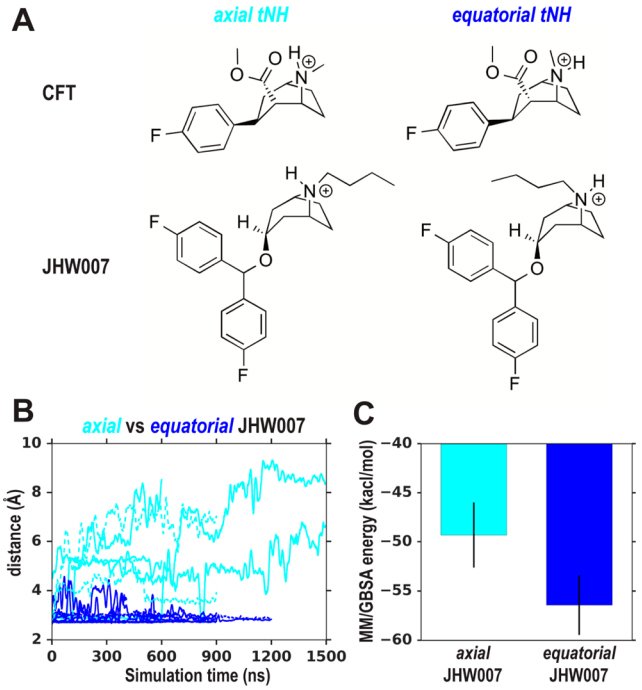

Figure 1. Equatorial tNH JHW007 is the more stable isoform in the hDAT S1 site. (A) Structures of CFT (top row) and JHW007 (bottom row). The axial tNH (left column) and equatorial tNH (right column) stereoisomers are shown. (B) Distance between the nitrogen of the tropane ring in JHW007 and the closest oxygen of the carbonyl group of Asp79 measured throughout all simulations for the axial (cyan) and equatorial (blue) tNH isoforms of JHW007 bound in WT hDAT. Results from the OPLS3 force field simulations are in dotted lines. (C) MM/GBSA binding energies of axial (cyan) and equatorial (blue) tNH JHW007 isomers bound in WT hDAT. Averages and standard deviations are shown for 500 Bayesian Markov model samples with 100 frames for each MS (of those that have >75% probability to belong to their respective MSs) derived from the simulations using CHARMM36/GAAMP force field.

substituents at position 3 of the tropane ring change the equilibrium between axial and equatorial tNH isomers, which in turn modulates their activity and selectivity for one monoamine transporter over another.[47] Interestingly, the cocaine and CFT bound crystal structures of dDAT (PDB IDs: 4XP4 and 4XPG, respectively) are both in an axial tNH conformation. Compared to cocaine and CFT, JHW007 lacks a carbonyl oxygen on the tropane ring that may interact with tNH.

We first docked axial and equatorial tNH JHW007 in the S1 site of our hDAT model (see Methods). The S1 site in DAT can be divided into subsites A, B, and C, as defined by Sørensen et al.[48] Interestingly, both axial and equatorial tNH JHW007 adopted similar binding modes—the positively charged amine forms a salt bridge interaction with Asp79 in subsite A, and the fluorophenyl rings are oriented in subsites B and C, but with different rotamers of the methoxy linker for the axial and equatorial forms. In comparison, in the crystal structures of dDAT bound with cocaine and CFT, the tropane moiety and a (fluoro)phenyl ring of these compounds occupy subsites A and B similarly to JHW007, but they do not protrude to subsite C as they lack the additional phenyl ring in JHW007.[24]

In our MD simulations of hDAT, the axial tNH JHW007 isomer was not stable in the S1 site and the interaction with Asp79 consistently broke, whereas the equatorial tNH of JHW007 consistently retained its interaction with Asp79 (Figure 1B). Such a drastic difference between the axial and equatorial tNH JHW007 isoforms is independent of the force field used, either the CHARMM36/GAAMP or the OPLS3 force field (see Methods and Table 1). Based on these MD simulations, we then carried out MM/GBSA calculations (see Methods) to estimate the ligand-binding affinities. Our results indicate that the equatorial tNH JHW007 is the preferred isomer in the S1 site with either of the force fields: for the frames from the simulations with the CHARMM36/GAAMP force field, the MM/GBSA binding energy for equatorial tNH JHW007 (−57.3 ± 2.7 kcal/mol) is 8.8 kcal/mol lower than that of axial tNH JHW007 (−48.4 ± 2.3 kcal/mol) (Figure 1C); for the frames from the simulations with the OPLS3 force field, those values are −78.6 ± 5.0 kcal/mol for the equatorial tNH JHW007 and −71.7 ± 6.0 kcal/mol for the axial tNH JHW007.

We then carried out quantum mechanical calculations of standalone CFT molecule in water and found that the energy difference between axial and equatorial tNH isoforms is 8.7 kcal/mol; in contrast, that for JHW007 is only 0.9 kcal/mol (Table 2). The results suggest that the axial isoform of CFT is

Table 2. Quantum Mechanical Potential Energies of Axial and Equatorial tNH Isoforms of CFT and JHW007[a]

	axial tNH (hartrees)	equatorial tNH (hartrees)	axial−equatorial (hartrees)	axial−equatorial (kcal/mol)
JHW007	−1262.1768	−1262.1753	−0.0015	−0.9
CFT	−927.2953	−927.2814	−0.0139	−8.7

[a]The calculations were performed using the DFT method with the (B3LYP) 6-31G** basis set in a water solvent.

significantly more dominant than its equatorial form, as the former is stabilized by an intramolecular hydrogen bond between tNH and the carbonyl oxygen on the 2-position of the tropane ring. In the absence of such an interaction in JHW007, the small energy difference between the two isoforms allows specific external interactions to easily switch the preference to the equatorial isoform, which is indeed what we observed in the binding site of hDAT in our MD simulations.

Thus, equatorial tNH JHW007 is the preferred isoform in binding to hDAT, and therefore we use this form for the following simulation and analysis, and refer to the complex as hDAT/JHW007.

MSM Analysis Identified Distinct Conformational States. Our MSM analysis of the conformational transitions and preferences in each of the six simulated conditions was based on a microstate discretization of the combined simulation set of all six conditions. In each MSM, these microstates were further lumped into metastable states (MSs) resulting in one

DOI: 10.1021/acschemneuro.7b00094
ACS Chem. Neurosci. 2017, 8, 1735−1746

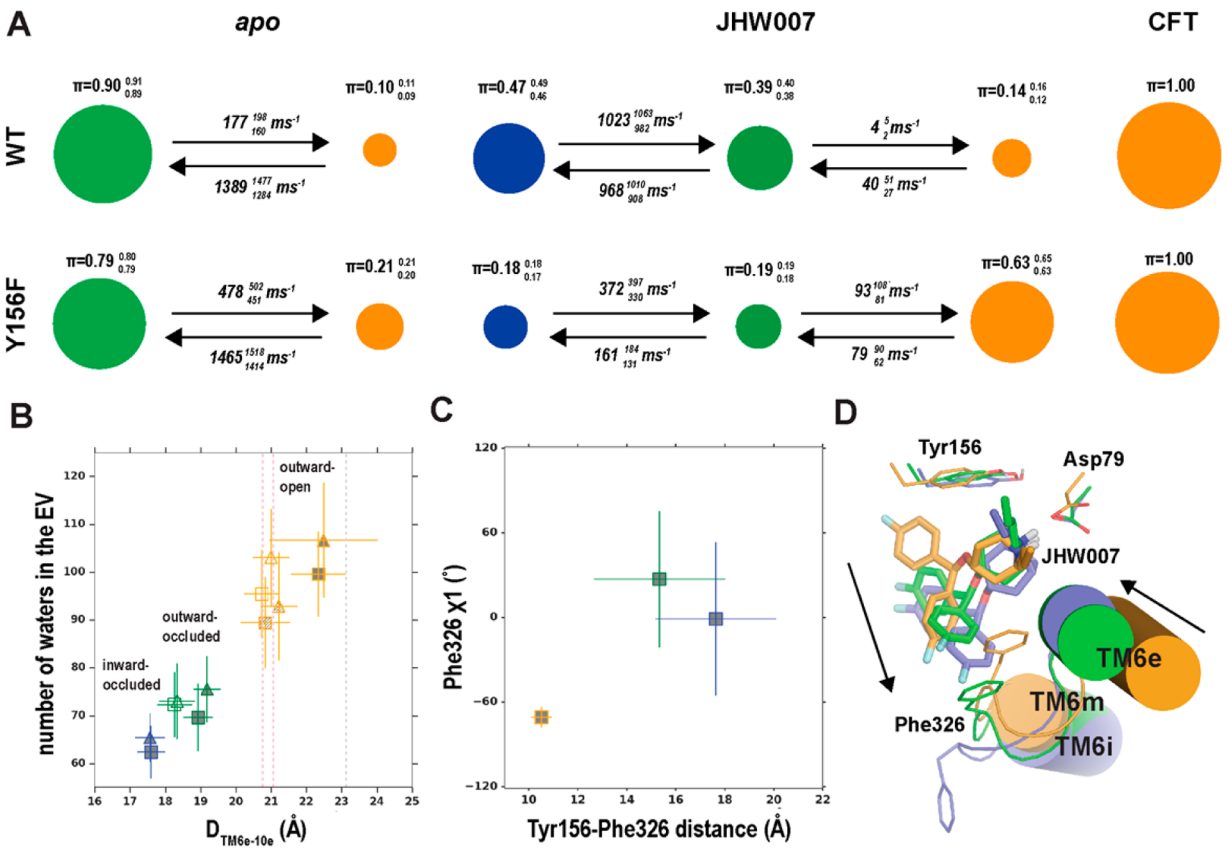

Figure 2. JHW007, CFT and the Y156F mutation shift hDAT to distinct conformational states. (A) Our MSM analysis identified three metastable states (MSs) that correspond to three conformations (outward-open (orange), outward-occluded (green), and inward-occluded (blue)). The area of each disk representing an MS is proportional to the equilibrium probability (π) in each simulated condition. The values from the maximum likelihood Bayesian Markov model and the upper and lower 1σ confidence intervals (in upper and lower cases, respectively) for π and transition rates from 500 Bayesian Markov model samples are shown. (B) Distances between the extracellular portions of TM6 and TM10 ($D_{TM6e\text{-}10e}$) are plotted against EV volumes (number of waters in EV) for each MS of each simulated condition. WT and Y156F mutant are represented by squares and triangles, whereas the *apo*, JHW007-bound and CFT-bound conditions are indicated by open, solid gray, and hatched fill styles, respectively. As references, the $D_{TM6e\text{-}10e}$s are also shown for the crystal structures of dDAT bound with CFT (PDB ID: 4XPG) and 3,4-dichlorophenylamine (DCP) (PDB IDs: 4XPA, 4XPH, 4XPT), which are in outward-open (gray dotted line) and "partially" occluded (pink dotted lines) conformations, respectively.[24] (C) Scatter plot of the distance between centers of mass (COM) of the aromatic rings of Tyr156 and Phe326, and the Phe326 χ_1 dihedral angle in each MS of the WT/JHW007 condition. (D) The downward movement of JHW007 in the S1 site is coordinated with the inward movement of TM6e from outward-open to outward-occluded and to inward-occluded conformation in the WT/JHW007 condition. Averages and standard deviations are shown for 500 Bayesian Markov model samples with 100 frames for each MS (of those that have >75% probability to belong to their respective MSs), in panels (B) and (C).

(for CFT-bound conditions), two (*apo* conditions), and three (JHW007-bound conditions) MSs (Figure 2A). Detailed methods of MD simulation setups and MSM analysis are described in the Methods.

In order to characterize the MSs, we quantified the extent of opening of the extracellular vestibule (EV) of hDAT by calculating the distance between the extracellular portions of TM6 and TM10 ($D_{TM6e\text{-}10e}$) (see Methods and below) as well as the volume of the EV, which was represented by the number of water molecules in the EV.[49,50] The MSs colored in orange in Figure 2, which are present in all conditions, have significantly larger $D_{TM6e\text{-}10e}$ and EV volume than the green and blue MSs (Figures 2), and are more outward-facing. As references, the $D_{TM6e\text{-}10e}$s are also calculated for the crystal structures of dDAT bound with CFT and DCP, which are in an outward-open and a "partially" occluded conformations, respectively[24] (Figure 2B). Because the difference in $D_{TM6e\text{-}10e}$ between the orange and green MSs (on average 2.8 Å for all simulated conditions) is larger than that between the dDAT/CFT and dDAT/DCP structures (2.2 Å), while the $D_{TM6e\text{-}10e}$ of orange MSs are similar to that of the dDAT/CFT structure, we designate the orange MSs as an outward-open conformation, the green MSs as an outward-occluded conformation, and blue MSs as an inward-occluded conformation (see below).

Y156F Mutation Shifts the hDAT Conformational Equilibrium to an Outward-Open Conformation. As the Y108F mutation in LeuT stabilizes an outward-open conformation,[21] we hypothesized that the aligned Y156F mutation in hDAT would promote an outward-open conformation as well. Indeed, our MSM analysis results indicate that the equilibrium probability of the outward-open conformation in the Y156F *apo* condition (21%) is significantly larger than that in the WT *apo* condition (10%) (Figure 2A). Thus, the Y156F mutation has a tendency to shift the transporter toward an outward-open conformation, which is also demonstrated by its enlarged EV compared to that of WT (Figure 2B). Furthermore, we observed that in 4 out of 9 Y156F/*apo* trajectories but none of WT/*apo* trajectories the Na^+ dissociates from the Na1 site, a trend that is consistent with our previous results of LeuT simulations, in which the absence

DOI: 10.1021/acschemneuro.7b00094
ACS Chem. Neurosci. 2017, 8, 1735−1746

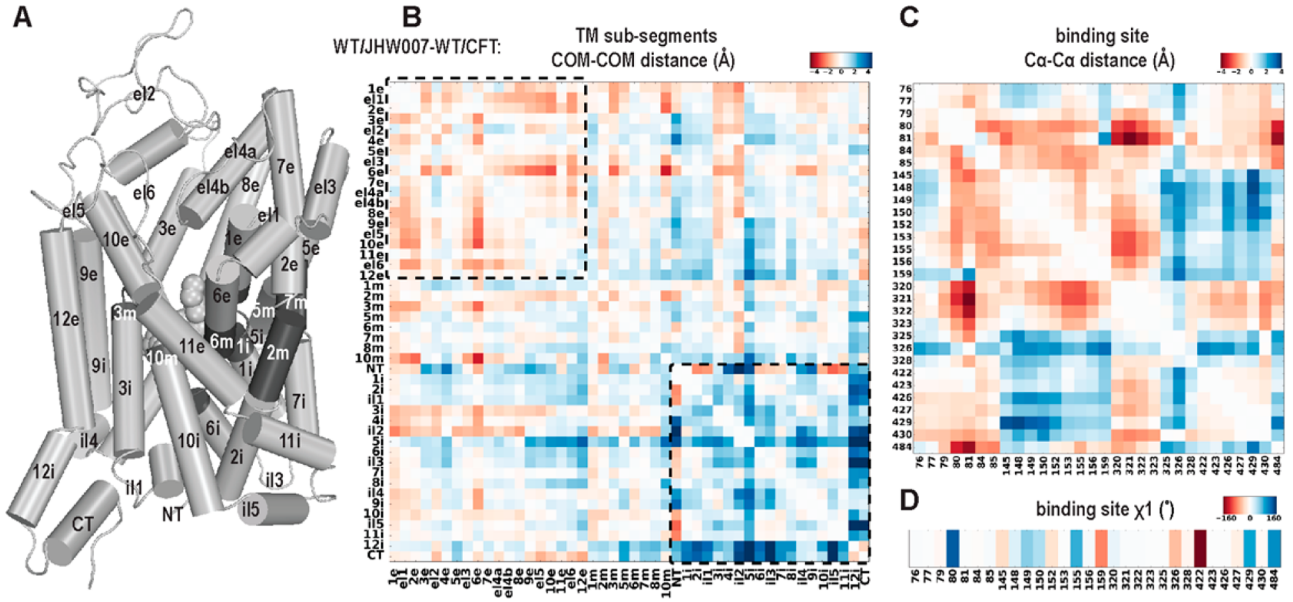

Figure 3. WT/JHW007 is less outward-facing and more inward-facing than WT/CFT. (A) The transmembrane helices in DAT are divided into extracellular ("e"), middle ("m", dark gray), and intracellular ("i") subsegments (see Methods). (B) The differences in the distances among TM subsegments highlight the less outward-facing and more inward-facing features of WT/JHW007 condition compared to WT/CFT. The differences of extracellular and intracellular subsegments are boxed in the upper left and lower right regions, respectively. For ligand binding residues, the distances between their Cα atoms (C) and the χ_1 dihedral angles of these residues (D) are compared. The results identified significant changes near Na1 and Na2 sites, i.e., the dark orange pixels near residues 81 and 321 in (C) for the Na1 site and the dark orange pixel for residue 422 in (D) for the Na2 site (see text). In these analyses by PIA-DAT, the dominant MSs of the WT/JHW007 and the WT/CFT conditions are used (see Methods). For (B)−(D), the color is scaled (see the color ramp for each panel) from blue to orange corresponding to higher and lower metric values, respectively, in the WT/JHW007 compared to the WT/CFT condition.

of Na1 is associated with a more outward-open conformation.[51] Together, these results demonstrate that disruption of the hydrogen bond between Tyr156 and Asp79 by the Y156F mutation in the *apo* conditions shifts hDAT toward an outward-open conformation.

JHW007 Shifts DAT Equilibrium toward an Inward-Occluded Conformation, whereas CFT Stabilizes the Outward-Open Conformation. As predicted from previous structure−function studies of hDAT[34,38] and the dDAT/CFT structure,[24] the outward-open conformation prevailed in our simulations of both the WT/CFT and Y156F/CFT conditions (Figure 2A). JHW007, on the other hand, induces hDAT to shift toward the blue MS, which is unique to the JHW007 bound conditions. As the $D_{TM6e\text{-}10e}$ of blue MSs is ∼1.1 Å shorter than that of the green MSs (Figure 2B), the blue MS likely represents an intermediate between the outward-occluded and inward-open conformations and we designate it as an inward-occluded conformation. Note this designation alone would be arbitrary because no dDAT structure has been solved in this conformation, however, based on our analysis (see below), it is a distinct and more inward-facing conformation compared to the outward-occluded conformation (green MS).

Based on our MSM analysis, this inward-occluded conformation has the highest equilibrium probability (47%) in the WT/JHW007 condition (Figure 2A). In Y156F/JHW007, the inward-occluded conformation is relatively less prevalent (18%) indicating that the Y156F mutation hampers the transporter from transitioning toward an inward-occluded conformation, in the presence of JHW007.

In WT/JHW007, from the outward-open to the outward-occluded and further to the inward-occluded conformation, there are coordinated changes between the diphenyl moiety of JHW007 and the phenyl ring of Phe326. The χ_1 rotamer changes of Phe326 are associated with an increased distance between Tyr156 and Phe326 (Figure 2C), which results in significant changes of the shape of the S1 site to accommodate the deeper binding pose of JHW007 (Figure 2D). The eventual rotation of Phe326 away from the S1 site is accompanied by a reconfiguration of the loop (TM6m) between TM6e and TM6i, and is coordinated with the inward-movement of TM6e (Figure 2D), which is the hallmark of the observed conformational transitions in our simulations. The aligned residues of Phe326, Phe259 in LeuT and Phe325 in dDAT, have been found to play an important role in both substrate and inhibitor binding.[23,52,53] Recently, a computational allosteric communication analysis identified that Phe259 was important for allosteric coupling between the S1 site and the intracellular gate region.[54] Our results are in line with these findings and highlight the importance of Phe326 in hDAT in transducing the impact of JHW007 to induce the overall conformational changes of hDAT.

We further quantified differences of a few structural features between the dominant conformations in the WT/JHW007 and WT/CFT conditions using the pairwise interaction analyzer for DAT (PIA-DAT) at both residue and subsegment levels (see Methods). Our analysis identified that the distances between extracellular subsegments of WT/CFT are generally larger (upper-left box in Figure 3B), i.e., more outward-facing, compared to the WT/JHW007 condition, with the most prominent change being the rearrangement of TM6e. We used $D_{TM6e\text{-}10e}$ to characterize different MSs (Figure 2B, see above). On the intracellular side, the increase in distances of the intracellular subsegments in WT/JHW007 compared to WT/

DOI: 10.1021/acschemneuro.7b00094
ACS Chem. Neurosci. 2017, 8, 1735−1746

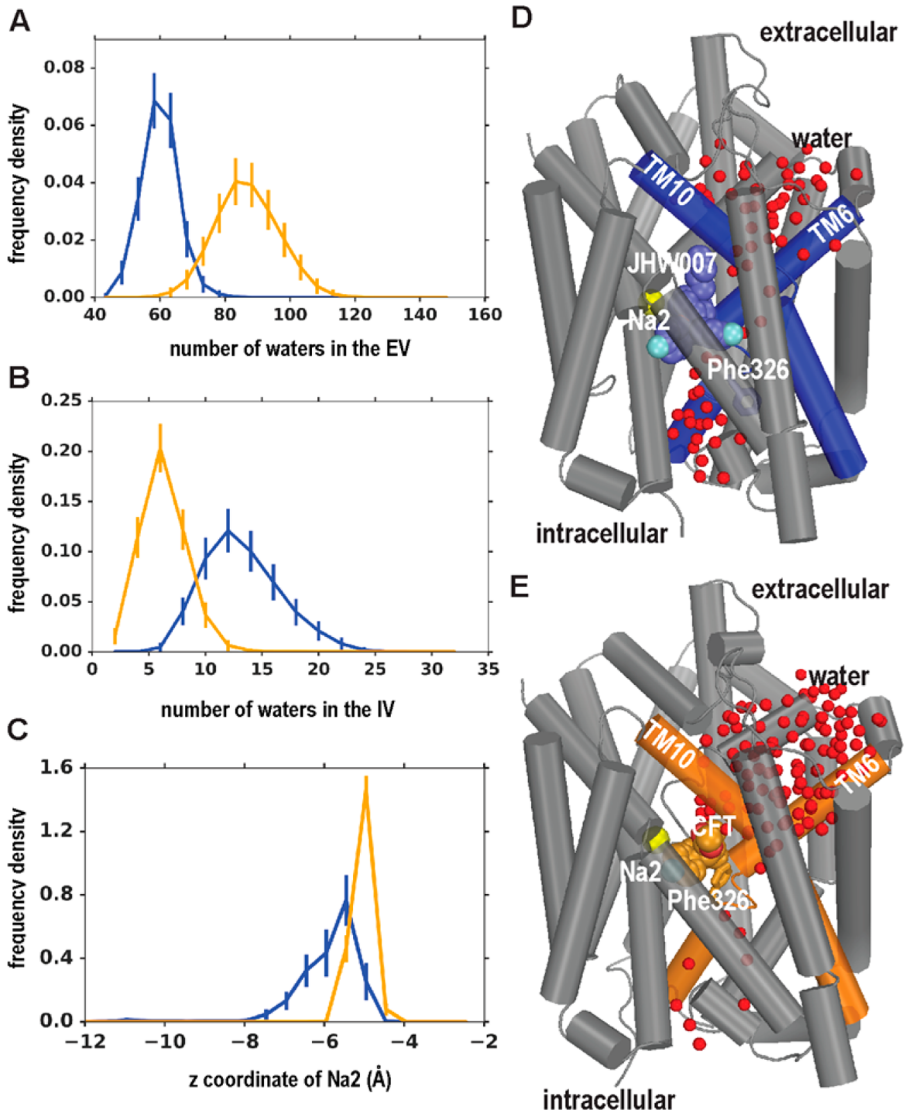

Figure 4. JHW007 and CFT stabilized hDAT in inward-occluded and outward-open conformations, respectively. Different trends of water penetrations in the extracellular (A), the intracellular (B) vestibules (EV and IV), and the *z* coordinate of Na2 (C) in the dominant MSs of the WT/JHW007 (blue) and the WT/CFT (orange) conditions indicate that JHW007 and CFT stabilize inward-occluded and outward-open hDAT conformations, respectively. Averages and standard deviations are shown for 500 Bayesian Markov model samples with 100 frames for each MS (of those that have >75% probability to belong to their respective MSs). Inward-occluded (D) and outward-open (E) hDAT conformations are shown in cylinder representations with water molecules in the EV and IV in red spheres, the ligands in blue (JHW007) and orange (CFT) spheres, Phe326 in sticks, and Na2 in yellow spheres. TM6 and 10 are highlighted with the colors corresponding to the MS in each panel.

CFT (lower-right box in Figure 3B) is consistent with WT/JHW007 being more inward-facing. The movement of TM5i toward lipids in WT/JHW007 is the most prominent change and contributes to the opening of the intracellular gate, as observed in our previous simulations with bacterial NSS homologues[55,56] (also see Discussion and Conclusions). In addition, PIA-DAT analysis revealed that the Cα-Cα distance between Ala81 and Ser321 (Ser321 is an Na1 coordinating residue) is larger in the WT/CFT condition (Figure 3C), which is likely correlated with Na1 having a tendency to dissociate from the Na1 site in this condition. Our PIA-DAT results also indicate a larger distance between Ile148 in TM3 and Ser429 in TM8, and the rotation of Ser429 side chain in the WT/JHW007 reflecting the accommodation of the diphenyl moiety of JHW007 (Figure 3C,D).

The transition from the outward-open to the inward-occluded conformation (Movie S1) would be expected to be accompanied by volume changes of the EV and the intracellular vestibule (IV). Indeed, from the analysis of the water counts in the WT/JHW007 condition, binding of JHW007 leads to closure of the EV and opening of the IV (Figure 4A,B), which eventually leads to water penetration from the IV to hydrate the JHW007 in the S1 site. In addition, the transition from an outward-facing to inward-occluded conformation is frequently accompanied by the dislocation of Na2 from its binding site (Figure 4C), which is accompanied by a change in the χ1 rotamer of Na2 coordinating Ser422 from *gauche*$^-$ to *gauche*$^+$ (Figure 3D).

Interestingly, the weak binding of the axial tNH JHW007 isomer in the S1 site was not able to induce the transporter to transition into an inward-occluded conformation (Figure S1). Taken together, the stable equatorial tNH isoform of JHW007 stabilizes a distinct hDAT conformation that lies between outward-occluded and inward-open conformations, which is

DOI: 10.1021/acschemneuro.7b00094
ACS Chem. Neurosci. 2017, 8, 1735−1746

Table 3. Binding Affinities at the WT and Y156F hDAT[a]

compd	DAT WT K_i (nM)	n	DAT Y156F K_i (nM)	n	Y156F:WT affinity ratio
CFT (K_d)	13.5 [12.2; 14.9]	21	25 [20; 31]	13	1.9
cocaine	223 [160; 309]	3	321 [235; 438]	3	1.4
JHW007	47 [33; 66]	3	260 [229; 296]	3	5.5

[a]Data taken from refs 33 and 61.

consistent with previous experimental results that JHW007 and other atypical inhibitors stabilize hDAT conformations that are more inward-facing than those stabilized by cocaine and its derivatives.[34,57]

DISCUSSION AND CONCLUSIONS

Many DAT inhibitors showing cocaine-like pharmacological and in vivo properties, such as cocaine, CFT, and RTI-55 (2*b*-carbomethoxy-3*b*-(4-iodophenyl)tropane),[58] all possess a hydrogen bond acceptor in the tropane ring that can stabilize their axial tNH conformation.[47] Interestingly, a BZT derivative, MFZ6-96,[59] which has a low K_i(Y156F)/K_i(WT) ratio, also has a carboxyl group in the tropane ring that stabilizes the axial tNH conformation. In contrast, the BZT derivatives with higher K_i(Y156F)/K_i(WT) ratio and atypical in vivo properties, such as JHW007 and GA 1-69[60] do not possess any axial tNH stabilizing group. Thus, our finding that JHW007 prefers the equatorial but not axial tNH isomer in the binding site of hDAT, and that this isomer stabilizes the transporter in an inward-occluded conformation, suggest specific ligand structure−function features that may differentiate atypical hDAT inhibitors.

By carrying out more than 36 μs of MD simulations in combination with MSM analysis, we sought to identify the preferred conformation of the hDAT WT and Y156F mutant in the absence of any ligand, or in the presence of either an atypical hDAT inhibitor (JHW007), or a cocaine derivative (CFT) in the S1 site. By integrating MSM analysis into our MD simulation procedure to restart trajectories based on undersampled microstates, we obtained convergence (Figures S2−S4) in delineating the energy landscape and kinetics of relevant conformational transitions, which we would have probably not been able to sample by simply performing 36 μs of conventional MD.

The comparisons between the hDAT WT/*apo* and Y156F/*apo* simulated conditions, and between WT/JHW007 and Y156F/JHW007, indicate that Y156F mutation in the S1 site shifts the transporter toward the outward-open conformation. By comparing WT/*apo*, WT/CFT, and Y156F/*apo*, we found that the binding of CFT shows an even stronger trend than Y156F mutation in stabilizing the transporter in the outward-open conformation. Thus, our results argue that the Tyr156-Asp79 interaction per se does not have a strong correlation with the conformations of the transporter, as it is present in the CFT stabilized outward-open conformation in the WT/CFT condition, whereas the Y156F/*apo* and Y156F/JHW007 conditions in its absence have large tendencies to be in the outward-open conformation than WT/*apo* and Y156F/JHW007, respectively. Rather, we propose that the phenotype of Y156F mutation in shifting the conformational equilibrium toward outward-open conformation is associated with the reduced mobility of its aromatic side chain in the S1 site. We found the χ1 rotamer of Tyr156 or Phe156 can only be in *trans* in the presence of a bound ligand (either CFT or JHW007), whereas in both WT/*apo* and Y156F/*apo* conditions, the χ1 rotamer of Tyr156 or Phe156 can also be in *gauche*$^-$; however, overall this rotamer populates 60.5% in *gauche*$^-$ in WT/*apo*, but 37.9% in Y156F/*apo*; in the orange states (outward-open conformation) of WT/*apo* and Y156F/*apo*, this differential trend is even more obvious, 58.9% in WT/*apo* and only 14.0% in Y156F/*apo*.

By comparing WT/*apo* and WT/JHW007, we found that JHW007 shifts the equilibrium in an opposite direction to the inward-occluded conformation. This novel inward-occluded conformation induced by JHW007 lies between outward-occluded and inward-open conformations. The higher equilibrium probability of this conformational state in the WT/JHW007 condition compared to Y156F/JHW007 condition suggests two competing driving forces in determining the conformational equilibrium in Y156F/JHW007: JHW007 shifts hDAT toward an inward-occluded conformation, whereas the Y156F mutation shifts it toward the outward-open conformation. This is consistent with previous mutagenesis studies showing that the binding affinity for JHW007 to the Y156F mutant is reduced compared to WT, whereas that for CFT is not affected (Table 3).[33,61]

In addition, JHW007 has been found to reduce accessibilities of the cysteines engineered at the Thr316 of TM6[62] in the EV compared to those in the presence of CFT, suggesting that JHW007 stabilizes a more occluded hDAT conformation. Interestingly, in the conformations revealed by our MD simulations and MSM analysis, Thr316 has smaller solvent accessible surface area (SASA) in the WT/JHW007 condition than in the WT/CFT condition (Figure S5), which is consistent with the experimental findings[62] and further validates the mechanistic relevance of the identified conformations in characterizing the molecular actions of these compounds on hDAT.

In the inward-occluded conformation, the hDAT binding site is at least partially occluded to the extracellular milieu. Thus, it is unlikely for JHW007 to bind directly to this conformation. Based on our results, we propose the recognition mechanism to be a combination of induced fit and conformational selection: JHW007 first binds to the green metastable state (the dominant state in the WT/apo condition), then it induces conformational transition to the blue, inward-occluded, state. From our results, we conclude that Y156F disrupts the conformational equilibrium but not the recognition mechanism.

The functions of hDAT are closely regulated by a variety of elements, and a growing number of DAT interaction proteins have been detected.[14,63−67] These interaction partners have been shown to alter DAT surface levels and modulate DAT specific functions, for which the specifically associated conformations of hDAT are yet to be revealed. We hypothesize that the functional impact of atypical hDAT inhibitors must go beyond the transporter protein per se by triggering different downstream cellular effects from those initiated by cocaine binding. Interestingly, a recent study by Zhang et al. shows that conformational changes in the serotonin transporter (SERT), a homologue of DAT, directly affect protein kinase G mediated

DOI: 10.1021/acschemneuro.7b00094
ACS Chem. Neurosci. 2017, 8, 1735−1746

phosphorylation of the transporter.[68] Specifically, it was demonstrated that the inward-open conformation of SERT provides accessibility for Thr276 in the intracellular portion of TM5 (TM5i) to be phosphorylated by a kinase. An examination of our hDAT simulations shows that whereas in the CFT-bound outward-open conformation TM5i is in a structured helical conformation, in the JHW007-bound inward-occluded conformation TM5i is partially unwound. Consequently, the residue that aligns to Thr276 of SERT, Thr261, is exposed to water environment in the JHW007-bound inward-occluded conformation, resulting in a higher SASA (Figure S5). In addition, as demonstrated by our PIA-DAT analysis (Figure 3B), the inward-facing conformation induced by binding of JHW007 propagated to the TM12i-CT region, the conformational changes of which have been associated with the interaction between hDAT and calmodulin kinase II.[67]

Taken together, our findings on potentially common features of the atypical inhibitors and the atomistic details in their interactions with hDAT shed lights on the molecular mechanisms of these inhibitors, which may eventually lead to design of effective medications to treat cocaine dependence.

METHODS

MD Simulations. The hDAT model used as the starting point for our MD simulations was constructed by homology modeling based on the dDAT/nortriptyline crystal structure (PDB ID 4M48[23]) using MODELER.[69] Two Na^+ and one Cl^- ions resolved in the crystal structure were also included in the model. The JHW007 and CFT were docked into the central binding site of the hDAT model using the induced-fit docking (IFD) protocol[70] implemented in the Schrödinger suite (release 2015-4). The MD simulation systems were prepared using VMD.[71] The all-atom simulations were carried out with our previously established protocols for NSS molecular systems.[50,72] Briefly, hDAT was placed into explicit 1-palmitoyl-2-oleoyl-*sn*-glycero-3-phosphocholine lipid bilayer (POPC) using the orientation of dDAT/nortriptyline structure (PDB ID 4M48) from the Orientation of Proteins in Membranes database.[73] Na^+ and Cl^- ions corresponding to 0.15 M concentration were added. The simulations were carried out using NAMD[74] with the CHARMM36 force field.[75,76] The ligand parameters were obtained through the GAAMP server[77] with the initial force field based on CHARMM general force field (CGenFF) assigned by ParamChem.[78] Simulations were performed with a cutoff of 12 Å for the nonbonded interactions, and the particle mesh Ewald method was used to evaluate long-range electrostatic effects. In the isothermal−isobaric (NPT) ensemble, constant temperature (310 K) was maintained with Langevin dynamics, and 1 atm constant pressure was achieved with the hybrid Nose-Hoover Langevin piston method[79] on an anisotropic flexible periodic cell, with a constant-ratio constraint applied on the lipid bilayer in the $X-Y$ plane. The systems were initially minimized for 6000 steps, then a time step of 1 fs was used for the first 200 ps, which was then increased to 2 fs for the rest of the simulations.

To demonstrate that the binding mode differences between axial and equatorial isoforms of JHW007 are force field independent, we carried out additional simulations using Desmond MD systems (D. E. Shaw Research, New York, NY) and OPLS3 force field[80] with the same simulation protocol described above.

MSM Analysis. The MSM analysis[40,81−84] was performed using the pyEMMA program (version 2.0.4[85,86]) as described previously.[41,87] In order to describe the conformational changes in hDAT upon the mutation and binding of ligands, interhelical distances of the extracellular portions of the core-TMs of "LeuT-fold" transporters, i.e. TMs 1, 3, 6, 8, and 10 were chosen for the input featurizer. These distances were calculated using centers of mass (COMs) of Cα atoms of the following residues: 89−92 (TM1), 169−172 (TM3), 308−311 (TM6), 405−408 (TM8), and 470−473 (TM10). Thus, a total of 10 distances were used as input coordinates.

For the combined data set of all simulated conditions, the slow linear subspace of the input coordinates was estimated by a time-lagged independent component analysis (TICA),[88,89] and its dimensionality was reduced by projecting on the three slowest TICA components (which represent 71% of the cumulative kinetic variance[90]). We then performed k-means clustering to discretize this simulated subspace into 100 cluster centers (microstates). For a range of numbers of microstates (50, 100, 200, 1000), we had estimated an MSM for each situation, and concluded that the 100-state MSM performs best based on two criteria. First, the 100-state MSM has the highest score in terms of the variational principle,[91,92] using cross-validation[93] (Table S1), which we adapted from the MSMBuilder package[94] (in the adaptation, in order to use kinetic variance[90] as a variational score, we changed $\Sigma_{i=1}^{m} \lambda_i$ to $\Sigma_{i=1}^{m} \lambda_i^2$ for the training score, where λ_i is the ith slowest eigenvalue and m is the number of eigenvalues). Second, the 100-state MSM shows better convergence of the implied time scales in terms of the lag time (Figures S2 and S6−S8).

We then divided this discretized combined data set by individual simulated conditions, from each of which we estimated a Bayesian Markov model.[95] Implied relaxation time scales (ITSs)[96] for the transitions between these clusters were obtained as a function of various lag times (Figure S2). The Bayesian sampling was employed to compute statistical uncertainties of 500 transition matrix samples at each lag time. Convergences of ITSs for all MSMs was achieved at a lag time of 120 ns, which we thus consistently use for all our analyses. The PCCA++ method[97] was then used on each model to lump the resulting microstates into MSs. The structural and kinetic analysis was performed on those microstates that have more than 75% of probability to belong to a particular MS. The transition rates shown in Figure 2A are inverse mean first passage times, which were computed as previously described,[98] and π represents the stationary equilibrium probability of a given MS.

The MSMs were validated using Chapman-Kolmogorov tests (Figure S3 and S4),[40] which showed that the MSMs estimated at 120 ns were consistent with the simulation data within the 95% confidence interval computed by 500 bootstrapped samples of trajectories.[99] Generally, the Chapman−Kolmogorov test checks if the MSM models estimated at lag time τ can be used to make predictions for the data at longer times $k\tau$ within statistical error, i.e., if eq 1 can be satisfied:

$$P(k\tau) = P^k(\tau) \tag{1}$$

where $P(\tau)$ is the transition matrix estimated from the data at lag time τ (the Markov model), and $P(k\tau)$ is the transition matrix estimated from the same data at longer lag times $k\tau$. In practice, we use $P(k\tau)$ and $P^k(\tau)$, respectively, to propagate probability starting from one of the metastable states, and measure how much probability ends up in each metastable state.

To adequately sample the conformational space explored by hDAT in various conditions, we analyzed the population of microstates throughout the simulations and restarted several rounds simulations from those microstates that have been sampled least frequently.[41]

Conformational Analysis. $D_{TM6e\text{-}10e}$ were calculated using centers of mass (COMs) of Cα atoms of TM6e and TM10e residues (see below) in hDAT, and the aligned 307−315 (TM6e) and 469−477 (TM10e) in dDAT. The volume of the EV and IV was measured by computing the number of water molecules in the vestibules as described in our previous studies.[49,50] Dihedral angle and solvent accessible surface area (SASA) were calculated with MDTraj (version 1.7.2)[100] in combination with *in-house* Python scripts. All conformational analyses were calculated from 500 Bayesian Markov model samples each with 100 frames sampled from those having >75% probability of belonging to each MS.

We developed the pairwise interaction analyzer for DAT (PIA-DAT), based on our previously developed PIA-GPCR.[101] The procedure and structural features measured by PIA-DAT are similar

DOI: 10.1021/acschemneuro.7b00094
ACS Chem. Neurosci. 2017, 8, 1735−1746

to PIA-GPCR described in[101] and to the distance difference matrices described in,[102] and systematically quantify conformational differences at both residue and subsegment levels. However, we took advantage of MSM analysis results in this study in the pairwise comparison of two compared conditions: the dominant MSs for each condition were chosen for the comparison; similar to other analyses in this study, for each MS, 500 Bayesian Markov model samples with 100 frames (of those that have >75% probability to belong to their respective MSs) were collected; the averages of structural features for each sample were then averaged as the inputs for PIA-DAT.

For the analysis of coarse-grained interaction network of hDAT, we defined the following structural elements: NT (N terminus, residues 58−64), TM1i (the intracellular section (i) of TM1, residues 65−74), TM1m (the middle section (m) of TM1, residues 75−82), TM1e (the extracellular section (e) of TM1, residues 83−92), EL1 (the extracellular loop 1, residues 93−95), TM2e (residues 96−101), TM2m (residues 102−111), TM2i (residues 112−124), IL1 (residues 125−135), TM3i (residues 136−151), TM3m (residues 152−156), TM3e (residues 157−172), EL2 (residues 173−237), TM4e (residues 238−246), TM4i (residues 247−255), IL2 (residues 256−261), TM5i (residues 262−266), TM5m (residues 267−274), TM5e (residues 275−284), EL3 (residues 285−307), TM6e (residues 308−316), TM6m (residues 317−328), TM6i (residues 329−335), IL3 (residues 336−342), TM7i (residues 343−352), TM7m (residues 353−359), TM7e (residues 360−374), EL4a (residues 375−386), EL4b (residues 387−404), TM8e (residues 405−417), TM8m (residues 418−426), TM8i (residues 427−436), IL4 (residues 437−441), TM9i (residues 445−454), TM9e (residues 455−465), EL5 (residues 466−469), TM10e (residues 470−478), TM10m (residues 479−483), TM10i (484−496), IL5 (residues 497−518), TM11i (residues 519−529), TM11e (residues 530−540), EL6 (residues 541−557), TM12e (residues 558−572), TM12i (residues 573−584), and CT (C terminus, residues 585−600).

The ligand binding site residues were determined to be those that are within 5 Å of ligand heavy atoms in >50% within the 500 Bayesian Markov model samples with 100 frames (of those that have >75% probability to belong to their respective MSs).

Quantum Mechanical and MM/GBSA Energy Calculations. Quantum mechanical geometry optimizations and potential energies of unbound JHW007 and CFT were obtained with DFT method using the B3LYP/6-31G** basis set and water solvent model within the Jaguar software[103] of the Schrodinger suite (release 2016-1).

An MM/GBSA analysis for the JHW007 binding modes simulated with the CHARMM36/GAAMP force field was performed using the protocol implemented in CHARMM (version 40b2)[104] using the GBSW implicit solvent model.[105] The frames used for this analysis were obtained from 500 Bayesian Markov model samples each with 100 frames sampled from those having >75% probability of belonging to the most stable MS in each of the conditions (i.e., blue and green MSs for equatorial and axial tNH JHW007, respectively). The MM/GBSA analysis for the JHW007 binding modes simulated with the OPLS3 force field was performed using the Thermal MM/GBSA module within the Schrodinger suite (release 2016−4), for the last 300 ns of each of the four OPLS3 trajectories with an interval of 3 ns.

■ ASSOCIATED CONTENT

Supporting Information

The Supporting Information is available free of charge on the ACS Publications website at DOI: 10.1021/acschemneuro.7b00094.

Conformational changes identified in the axial tNH JHW007-bound WT hDAT condition; implied time scales for 100 microstate MSMs; Chapman−Kolmogorov tests of WT and Y156F conditions; structural differences and SASA values for residues Thr316 and Thr261; implied time scales for 50, 200, and 1000 microstate MSMs; variational scores for a range of microstates (PDF)

Conformational transitions in the WT/JHW007 condition (MPG)

■ AUTHOR INFORMATION

Corresponding Author

*Mailing address: 333 Cassell Drive, Room 1121, Baltimore, MD 21224. Telephone: 443-740-2774. E-mail: lei.shi2@nih.gov.

ORCID

Lei Shi: 0000-0002-4137-096X

Author Contributions

A.M.A. and L.S. designed the study. A.M.A., S.S., Z.L., F.N., and L.S. carried out the computations and analysis. All the authors took part in interpreting the results. A.M.A. and L.S. wrote the initial draft, with S.S. and F.N. participating in revising the manuscript. All authors have given approval to the final version of the manuscript.

Funding

Support for this research was provided to A.M.A. and L.S. by the Intramural Research Program of National Institutes of Health (NIH), National Institute on Drug Abuse. S.S. is supported by a DRS/Marie Curie Post-Doctoral POINT Fellowship of Freie Universität Berlin.

Notes

The authors declare no competing financial interest.

■ ACKNOWLEDGMENTS

We thank Dr. Amy H. Newman for insightful discussion. We also thank Dr. Min Xu for his help with the variational score. This work utilized the computational resources of the NIH HPC Biowulf cluster (http://hpc.nih.gov).

■ REFERENCES

(1) Kristensen, A. S., Andersen, J., Jorgensen, T. N., Sorensen, L., Eriksen, J., Loland, C. J., Stromgaard, K., and Gether, U. (2011) SLC6 neurotransmitter transporters: structure, function, and regulation. *Pharmacol Rev. 63*, 585−640.

(2) Felten, A., Montag, C., Markett, S., Walter, N. T., and Reuter, M. (2011) Genetically determined dopamine availability predicts disposition for depression. *Brain and Behavior 1*, 109−118.

(3) Gainetdinov, R. R., and Caron, M. G. (2003) Monoamine transporters: from genes to behavior. *Annu. Rev. Pharmacol. Toxicol. 43*, 261−284.

(4) Kurian, M. A., Zhen, J., Cheng, S.-Y., Li, Y., Mordekar, S. R., Jardine, P., Morgan, N. V., Meyer, E., Tee, L., Pasha, S., et al. (2009) Homozygous loss-of-function mutations in the gene encoding the dopamine transporter are associated with infantile parkinsonism-dystonia. *J. Clin. Invest. 119*, 1595−1603.

(5) Chen, R., Tilley, M. R., Wei, H., Zhou, F., Zhou, F. M., Ching, S., Quan, N., Stephens, R. L., Hill, E. R., Nottoli, T., Han, D. D., and Gu, H. H. (2006) Abolished cocaine reward in mice with a cocaine-insensitive dopamine transporter. *Proc. Natl. Acad. Sci. U. S. A. 103*, 9333−9338.

(6) Torres, G. E., and Amara, S. G. (2007) Glutamate and monoamine transporters: new visions of form and function. *Curr. Opin. Neurobiol. 17*, 304−312.

(7) Chen, N.-H., Reith, M. E., and Quick, M. W. (2004) Synaptic uptake and beyond: the sodium-and chloride-dependent neurotransmitter transporter family SLC6. *Pfluegers Arch. 447*, 519−531.

(8) Volkow, N. D., Wang, G. J., Fischman, M. W., Foltin, R. W., Fowler, J. S., Abumrad, N. N., Vitkun, S., Logan, J., Gatley, S. J., Pappas, N., Hitzemann, R., and Shea, C. E. (1997) Relationship between subjective effects of cocaine and dopamine transporter occupancy. *Nature 386*, 827−830.

DOI: 10.1021/acschemneuro.7b00094
ACS Chem. Neurosci. 2017, 8, 1735−1746

(9) Ritz, M. C., Lamb, R. J., Goldberg, S. R., and Kuhar, M. J. (1987) Cocaine receptors on dopamine transporters are related to self-administration of cocaine. *Science 237*, 1219−1223.
(10) Bergman, J., Madras, B. K., Johnson, S. E., and Spealman, R. (1989) Effects of cocaine and related drugs in nonhuman primates. III. Self-administration by squirrel monkeys. *J. Pharmacol. Exp. Ther. 251*, 150−155.
(11) Cline, E. J., Scheffel, U., Boja, J. W., Mitchell, W. M., Carroll, F. I., Abraham, P., Lewin, A. H., and Kuhar, M. J. (1992) In vivo binding of [125I]RTI-55 to dopamine transporters: pharmacology and regional distribution with autoradiography. *Synapse 12*, 37−46.
(12) Tanda, G., Newman, A. H., and Katz, J. L. (2009) Discovery of drugs to treat cocaine dependence: behavioral and neurochemical effects of atypical dopamine transport inhibitors. *Adv. Pharmacol. 57*, 253−289.
(13) Newman, A. H., and Katz, J. L. (2009) Atypical Dopamine Uptake Inhibitors that Provide Clues About Cocaine's Mechanism at the Dopamine Transporter. In *Transporters as Targets for Drugs* (Napier, S., and Bingham, M., Eds.), pp 95−129, Springer, Berlin, Heidelberg.
(14) Reith, M. E., Blough, B. E., Hong, W. C., Jones, K. T., Schmitt, K. C., Baumann, M. H., Partilla, J. S., Rothman, R. B., and Katz, J. L. (2015) Behavioral, biological, and chemical perspectives on atypical agents targeting the dopamine transporter. *Drug Alcohol Depend. 147*, 1−19.
(15) Desai, R. I., Kopajtic, T. A., Koffarnus, M., Newman, A. H., and Katz, J. L. (2005) Identification of a dopamine transporter ligand that blocks the stimulant effects of cocaine. *J. Neurosci. 25*, 1889−1893.
(16) Hiranita, T., Soto, P. L., Newman, A. H., and Katz, J. L. (2009) Assessment of reinforcing effects of benztropine analogs and their effects on cocaine self-administration in rats: comparisons with monoamine uptake inhibitors. *J. Pharmacol. Exp. Ther. 329*, 677−686.
(17) Zomot, E., Bendahan, A., Quick, M., Zhao, Y., Javitch, J. A., and Kanner, B. I. (2007) Mechanism of chloride interaction with neurotransmitter:sodium symporters. *Nature 449*, 726−730.
(18) Jardetzky, O. (1966) Simple allosteric model for membrane pumps. *Nature 211*, 969−970.
(19) Zhao, C., and Noskov, S. Y. (2013) The molecular mechanism of ion-dependent gating in secondary transporters. *PLoS Comput. Biol. 9*, e1003296.
(20) Kazmier, K., Sharma, S., Islam, S. M., Roux, B., and Mchaourab, H. S. (2014) Conformational cycle and ion-coupling mechanism of the Na+/hydantoin transporter Mhp1. *Proc. Natl. Acad. Sci. U. S. A. 111*, 14752−14757.
(21) Krishnamurthy, H., and Gouaux, E. (2012) X-ray structures of LeuT in substrate-free outward-open and apo inward-open states. *Nature 481*, 469−474.
(22) Yamashita, A., Singh, S. K., Kawate, T., Jin, Y., and Gouaux, E. (2005) Crystal structure of a bacterial homologue of Na+/Cl–dependent neurotransmitter transporters. *Nature 437*, 215−223.
(23) Penmatsa, A., Wang, K. H., and Gouaux, E. (2013) X-ray structure of dopamine transporter elucidates antidepressant mechanism. *Nature 503*, 85−90.
(24) Wang, K. H., Penmatsa, A., and Gouaux, E. (2015) Neurotransmitter and psychostimulant recognition by the dopamine transporter. *Nature 521*, 322−327.
(25) Cheng, M. H., and Bahar, I. (2015) Molecular mechanism of dopamine transport by human dopamine transporter. *Structure 23*, 2171−2181.
(26) Forrest, L. R., Zhang, Y. W., Jacobs, M. T., Gesmonde, J., Xie, L., Honig, B. H., and Rudnick, G. (2008) Mechanism for alternating access in neurotransmitter transporters. *Proc. Natl. Acad. Sci. U. S. A. 105*, 10338−10343.
(27) Shan, J., Javitch, J. A., Shi, L., and Weinstein, H. (2011) The substrate-driven transition to an inward-facing conformation in the functional mechanism of the dopamine transporter. *PLoS One 6*, e16350.
(28) Khelashvili, G., Stanley, N., Sahai, M. A., Medina, J., LeVine, M. V., Shi, L., De Fabritiis, G., and Weinstein, H. (2015) Spontaneous Inward Opening of the Dopamine Transporter Is Triggered by PIP-Regulated Dynamics of the N-Terminus. *ACS Chem. Neurosci. 6*, 1825.
(29) Borre, L., Andreassen, T. F., Shi, L., Weinstein, H., and Gether, U. (2014) The second sodium site in the dopamine transporter controls cation permeation and is regulated by chloride. *J. Biol. Chem. 289*, 25764−25773.
(30) Hong, W. C., Kopajtic, T. A., Xu, L., Lomenzo, S. A., Jean, B., Madura, J. D., Surratt, C. K., Trudell, M. L., and Katz, J. L. (2016) 2-Substituted 3β-Aryltropane Cocaine Analogs Produce Atypical Effects without Inducing Inward-Facing Dopamine Transporter Conformations. *J. Pharmacol. Exp. Ther. 356*, 624−634.
(31) Stockner, T., Montgomery, T. R., Kudlacek, O., Weissensteiner, R., Ecker, G. F., Freissmuth, M., and Sitte, H. H. (2013) Mutational analysis of the high-affinity zinc binding site validates a refined human dopamine transporter homology model. *PLoS Comput. Biol. 9*, e1002909.
(32) Yuan, Y., Quizon, P. M., Sun, W.-L., Yao, J., Zhu, J., and Zhan, C.-G. (2016) Role of Histidine 547 of Human Dopamine Transporter in Molecular Interaction with HIV-1 Tat and Dopamine Uptake. *Sci. Rep. 6*, 27314−27314.
(33) Beuming, T., Kniazeff, J., Bergmann, M. L., Shi, L., Gracia, L., Raniszewska, K., Newman, A. H., Javitch, J. A., Weinstein, H., Gether, U., and Loland, C. J. (2008) The binding sites for cocaine and dopamine in the dopamine transporter overlap. *Nat. Neurosci. 11*, 780−789.
(34) Loland, C. J., Desai, R. I., Zou, M. F., Cao, J., Grundt, P., Gerstbrein, K., Sitte, H. H., Newman, A. H., Katz, J. L., and Gether, U. (2008) Relationship between conformational changes in the dopamine transporter and cocaine-like subjective effects of uptake inhibitors. *Mol. Pharmacol. 73*, 813−823.
(35) Reith, M. E., Berfield, J. L., Wang, L. C., Ferrer, J. V., and Javitch, J. A. (2001) The uptake inhibitors cocaine and benztropine differentially alter the conformation of the human dopamine transporter. *J. Biol. Chem. 276*, 29012−29018.
(36) Loland, C. J., Norregaard, L., Litman, T., and Gether, U. (2002) Generation of an activating Zn(2+) switch in the dopamine transporter: mutation of an intracellular tyrosine constitutively alters the conformational equilibrium of the transport cycle. *Proc. Natl. Acad. Sci. U. S. A. 99*, 1683−1688.
(37) Loland, C. J., Granas, C., Javitch, J. A., and Gether, U. (2004) Identification of intracellular residues in the dopamine transporter critical for regulation of transporter conformation and cocaine binding. *J. Biol. Chem. 279*, 3228−3238.
(38) Bisgaard, H., Larsen, M. A., Mazier, S., Beuming, T., Newman, A. H., Weinstein, H., Shi, L., Loland, C. J., and Gether, U. (2011) The binding sites for benztropines and dopamine in the dopamine transporter overlap. *Neuropharmacology 60*, 182−190.
(39) Bowman, G. R., Pande, V. S., and Noé, F. (2013) *An introduction to markov state models and their application to long timescale molecular simulation*, Vol. *797*, Springer Science & Business Media.
(40) Prinz, J.-H., Wu, H., Sarich, M., Keller, B., Senne, M., Held, M., Chodera, J. D., Schütte, C., and Noé, F. (2011) Markov models of molecular kinetics: Generation and validation. *J. Chem. Phys. 134*, 174105.
(41) Plattner, N., and Noé, F. (2015) Protein conformational plasticity and complex ligand-binding kinetics explored by atomistic simulations and Markov models. *Nat. Commun. 6*, 7653.
(42) Kohlhoff, K. J., Shukla, D., Lawrenz, M., Bowman, G. R., Konerding, D. E., Belov, D., Altman, R. B., and Pande, V. S. (2014) Cloud-based simulations on Google Exacycle reveal ligand modulation of GPCR activation pathways. *Nat. Chem. 6*, 15−21.
(43) Silva, D.-A., Bowman, G. R., Sosa-Peinado, A., and Huang, X. (2011) A role for both conformational selection and induced fit in ligand binding by the LAO protein. *PLoS Comput. Biol. 7*, e1002054.
(44) Gu, S., Silva, D.-A., Meng, L., Yue, A., and Huang, X. (2014) Quantitatively characterizing the ligand binding mechanisms of choline binding protein using Markov state model analysis. *PLoS Comput. Biol. 10*, e1003767.

DOI: 10.1021/acschemneuro.7b00094
ACS Chem. Neurosci. 2017, 8, 1735−1746

(45) Buch, I., Giorgino, T., and De Fabritiis, G. (2011) Complete reconstruction of an enzyme-inhibitor binding process by molecular dynamics simulations. *Proc. Natl. Acad. Sci. U. S. A. 108*, 10184−10189.
(46) Razavi, A. M., Khelashvili, G., and Weinstein, H. (2017) A Markov State-based Quantitative Kinetic Model of Sodium Release from the Dopamine Transporter. *Sci. Rep. 7*, 40076.
(47) Krunić, A., Pan, D., Dunn, W. J., and Mariappan, S. S. (2009) The stereochemistry of N-methyl and aryl substituents determine the biological activities of 3-aryl-8-methyl-8-azabicyclo [3.2. 1] oct-2, 3-enes. *Bioorg. Med. Chem. 17*, 811−819.
(48) Sørensen, L., Andersen, J., Thomsen, M., Hansen, S. M., Zhao, X., Sandelin, A., Strømgaard, K., and Kristensen, A. S. (2012) Interaction of antidepressants with the serotonin and norepinephrine transporters mutational studies of the s1 substrate binding pocket. *J. Biol. Chem. 287*, 43694−43707.
(49) Stolzenberg, S., Khelashvili, G., and Weinstein, H. (2012) Structural intermediates in a model of the substrate translocation path of the bacterial glutamate transporter homologue GltPh. *J. Phys. Chem. B 116*, 5372−5383.
(50) Stolzenberg, S., Quick, M., Zhao, C., Gotfryd, K., Khelashvili, G., Gether, U., Loland, C. J., Javitch, J. A., Noskov, S., Weinstein, H., and Shi, L. (2015) Mechanism of the Association between Na+ Binding and Conformations at the Intracellular Gate in Neurotransmitter:Sodium Symporters. *J. Biol. Chem. 290*, 13992−14003.
(51) Zhao, C., Stolzenberg, S., Gracia, L., Weinstein, H., Noskov, S., and Shi, L. (2012) Ion-Controlled Conformational Dynamics in the Outward-Open Transition from an Occluded State of LeuT. *Biophys. J. 103*, 878−888.
(52) Singh, S. K., Piscitelli, C. L., Yamashita, A., and Gouaux, E. (2008) A competitive inhibitor traps LeuT in an open-to-out conformation. *Science 322*, 1655−1661.
(53) Penmatsa, A., Wang, K. H., and Gouaux, E. (2015) X-ray structures of Drosophila dopamine transporter in complex with nisoxetine and reboxetine. *Nat. Struct. Mol. Biol. 22*, 506−508.
(54) LeVine, M. V., and Weinstein, H. (2014) NbIT–a new information theory-based analysis of allosteric mechanisms reveals residues that underlie function in the leucine transporter LeuT. *PLoS Comput. Biol. 10*, e1003603.
(55) Shi, L., and Weinstein, H. (2010) Conformational rearrangements to the intracellular open states of the LeuT and ApcT transporters are modulated by common mechanisms. *Biophys. J. 99*, L103−L105.
(56) Billesbølle, C. B., Krüger, M. B., Shi, L., Quick, M., Li, Z., Stolzenberg, S., Kniazeff, J., Gotfryd, K., Mortensen, J. S., Javitch, J. A., et al. (2015) Substrate-induced unlocking of the inner gate determines the catalytic efficiency of a neurotransmitter: sodium symporter. *J. Biol. Chem. 290*, 26725−26738.
(57) Tanda, G., Li, S. M., Mereu, M., Thomas, A. M., Ebbs, A. L., Chun, L. E., Tronci, V., Green, J. L., Zou, M.-F., Kopajtic, T. A., et al. (2013) Relations between stimulation of mesolimbic dopamine and place conditioning in rats produced by cocaine or drugs that are tolerant to dopamine transporter conformational change. *Psychopharmacology 229*, 307−321.
(58) Carroll, F. I., Gao, Y., Rahman, M. A., Abraham, P., Parham, K., Lewin, A. H., Boja, J. W., and Kuhar, M. J. (1991) Synthesis, ligand binding, QSAR, and CoMFA study of 3. beta.-(p-substituted phenyl) tropane-2. beta.-carboxylic acid methyl esters. *J. Med. Chem. 34*, 2719−2725.
(59) Zou, M.-F., Cao, J., Kopajtic, T., Desai, R. I., Katz, J. L., and Newman, A. H. (2006) Structure-activity relationship studies on a novel series of (S)-2β-substituted 3α-[bis (4-fluoro-or 4-chlorophenyl) methoxy] tropane analogues for in vivo investigation. *J. Med. Chem. 49*, 6391−6399.
(60) Li, S.-M., Kopajtic, T. A., O'Callaghan, M. J., Agoston, G. E., Cao, J., Newman, A. H., and Katz, J. L. (2011) N-substituted benztropine analogs: selective dopamine transporter ligands with a fast onset of action and minimal cocaine-like behavioral effects. *J. Pharmacol. Exp. Ther. 336*, 575−585.
(61) Cao, J., Slack, R. D., Bakare, O. M., Burzynski, C., Rais, R., Slusher, B. S., Kopajtic, T., Bonifazi, A., Ellenberger, M. P., and Yano, H. (2016) Novel and High Affinity 2-[(Diphenylmethyl) sulfinyl] acetamide (Modafinil) Analogues as Atypical Dopamine Transporter Inhibitors. *J. Med. Chem. 59*, 10676−10691.
(62) Hiranita, T., Wilkinson, D. S., Hong, W. C., Zou, M.-F., Kopajtic, T. A., Soto, P. L., Lupica, C. R., Newman, A. H., and Katz, J. L. (2014) 2-isoxazol-3-phenyltropane derivatives of cocaine: molecular and atypical system effects at the dopamine transporter. *J. Pharmacol. Exp. Ther. 349*, 297−309.
(63) Hadlock, G. C., Nelson, C. C., Baucum, A. J., Hanson, G. R., and Fleckenstein, A. E. (2011) Ex vivo identification of protein−protein interactions involving the dopamine transporter. *J. Neurosci. Methods 196*, 303−307.
(64) Eriksen, J., Jørgensen, T. N., and Gether, U. (2010) Regulation of dopamine transporter function by protein-protein interactions: new discoveries and methodological challenges. *J. Neurochem. 113*, 27−41.
(65) Cervinski, M. A., Foster, J. D., and Vaughan, R. A. (2005) Psychoactive substrates stimulate dopamine transporter phosphorylation and down-regulation by cocaine-sensitive and protein kinase C-dependent mechanisms. *J. Biol. Chem. 280*, 40442−40449.
(66) Sorkina, T., Richards, T. L., Rao, A., Zahniser, N. R., and Sorkin, A. (2009) Negative regulation of dopamine transporter endocytosis by membrane-proximal N-terminal residues. *J. Neurosci. 29*, 1361−1374.
(67) Fog, J. U., Khoshbouei, H., Holy, M., Owens, W. A., Vaegter, C. B., Sen, N., Nikandrova, Y., Bowton, E., McMahon, D. G., Colbran, R. J., et al. (2006) Calmodulin kinase II interacts with the dopamine transporter C terminus to regulate amphetamine-induced reverse transport. *Neuron 51*, 417−429.
(68) Zhang, Y.-W., Turk, B. E., and Rudnick, G. (2016) Control of serotonin transporter phosphorylation by conformational state. *Proc. Natl. Acad. Sci. U. S. A. 113*, E2776−E2783.
(69) John, B., and Sali, A. (2003) Comparative protein structure modeling by iterative alignment, model building and model assessment. *Nucleic Acids Res. 31*, 3982−3992.
(70) Sherman, W., Beard, H. S., and Farid, R. (2006) Use of an induced fit receptor structure in virtual screening. *Chem. Biol. Drug Des. 67*, 83−84.
(71) Humphrey, W., Dalke, A., and Schulten, K. (1996) VMD: visual molecular dynamics. *J. Mol. Graphics 14* (33−38), 27−38.
(72) Shi, L., Quick, M., Zhao, Y., Weinstein, H., and Javitch, J. A. (2008) The mechanism of a neurotransmitter:sodium symporter–inward release of Na+ and substrate is triggered by substrate in a second binding site. *Mol. Cell 30*, 667−677.
(73) Lomize, M. A., Lomize, A. L., Pogozheva, I. D., and Mosberg, H. I. (2006) OPM: orientations of proteins in membranes database. *Bioinformatics 22*, 623−625.
(74) Phillips, J. C., Braun, R., Wang, W., Gumbart, J., Tajkhorshid, E., Villa, E., Chipot, C., Skeel, R. D., Kale, L., and Schulten, K. (2005) Scalable molecular dynamics with NAMD. *J. Comput. Chem. 26*, 1781−1802.
(75) MacKerell, A. D., Bashford, D., Bellott, Dunbrack, R. L., Evanseck, J. D., Field, M. J., Fischer, S., Gao, J., Guo, H., Ha, S., Joseph-McCarthy, D., Kuchnir, L., Kuczera, K., Lau, F. T. K., Mattos, C., Michnick, S., Ngo, T., Nguyen, D. T., Prodhom, B., Reiher, W. E., Roux, B., Schlenkrich, M., Smith, J. C., Stote, R., Straub, J., Watanabe, M., Wiórkiewicz-Kuczera, J., Yin, D., and Karplus, M. (1998) All-Atom Empirical Potential for Molecular Modeling and Dynamics Studies of Proteins†. *J. Phys. Chem. B 102*, 3586−3616.
(76) Best, R. B., Zhu, X., Shim, J., Lopes, P. E., Mittal, J., Feig, M., and MacKerell, A. D., Jr (2012) Optimization of the additive CHARMM all-atom protein force field targeting improved sampling of the backbone ϕ, ψ and side-chain χ1 and χ2 dihedral angles. *J. Chem. Theory Comput. 8*, 3257−3273.
(77) Huang, L., and Roux, B. (2013) Automated force field parameterization for nonpolarizable and polarizable atomic models based on ab initio target data. *J. Chem. Theory Comput. 9*, 3543−3556.
(78) Vanommeslaeghe, K., Hatcher, E., Acharya, C., Kundu, S., Zhong, S., Shim, J., Darian, E., Guvench, O., Lopes, P., Vorobyov, I.,

DOI: 10.1021/acschemneuro.7b00094
ACS Chem. Neurosci. 2017, 8, 1735−1746

and Mackerell, a. D. (2010) CHARMM general force field: A force field for drug-like molecules compatible with the CHARMM all-atom additive biological force fields. *J. Comput. Chem. 31*, 671−690.
(79) Feller, S. E., Zhang, Y., Pastor, R. W., and Brooks, B. R. (1995) Constant pressure molecular dynamics simulation: The Langevin piston method. *J. Chem. Phys. 103*, 4613−4621.
(80) Harder, E., Damm, W., Maple, J., Wu, C., Reboul, M., Xiang, J. Y., Wang, L., Lupyan, D., Dahlgren, M. K., and Knight, J. L. (2016) OPLS3: a force field providing broad coverage of drug-like small molecules and proteins. *J. Chem. Theory Comput. 12*, 281−296.
(81) Chodera, J. D., Singhal, N., Pande, V. S., Dill, K. A., and Swope, W. C. (2007) Automatic discovery of metastable states for the construction of Markov models of macromolecular conformational dynamics. *J. Chem. Phys. 126*, 155101.
(82) Noé, F., Horenko, I., Schütte, C., and Smith, J. C. (2007) Hierarchical analysis of conformational dynamics in biomolecules: transition networks of metastable states. *J. Chem. Phys. 126*, 155102.
(83) Buchete, N.-V., and Hummer, G. (2008) Coarse master equations for peptide folding dynamics. *J. Phys. Chem. B 112*, 6057−6069.
(84) Schütte, C. (1998) Conformational dynamics: modelling, theory, algorithm, and application to biomolecules. Habilitation dissertation, Free University Berlin.
(85) Scherer, M. K., Trendelkamp-Schroer, B., Paul, F., Pérez-Hernández, G., Hoffmann, M., Plattner, N., Wehmeyer, C., Prinz, J.-H., and Noé, F. (2015) PyEMMA 2: A software package for estimation, validation, and analysis of Markov models. *J. Chem. Theory Comput. 11*, 5525−5542.
(86) Senne, M., Trendelkamp-Schroer, B., Mey, A. S., Schütte, C., and Noé, F. (2012) EMMA: A software package for Markov model building and analysis. *J. Chem. Theory Comput. 8*, 2223−2238.
(87) Wieczorek, M., Sticht, J., Stolzenberg, S., Günther, S., Wehmeyer, C., El Habre, Z., Alvaro-Benito, M., Noé, F., and Freund, C. (2016) MHC class II complexes sample intermediate states along the peptide exchange pathway. *Nat. Commun. 7*, 13224.
(88) Pérez-Hernández, G., Paul, F., Giorgino, T., De Fabritiis, G., and Noé, F. (2013) Identification of slow molecular order parameters for Markov model construction. *J. Chem. Phys. 139*, 015102.
(89) Schwantes, C. R., and Pande, V. S. (2013) Improvements in Markov state model construction reveal many non-native interactions in the folding of NTL9. *J. Chem. Theory Comput. 9*, 2000−2009.
(90) Noé, F., and Clementi, C. (2015) Kinetic distance and kinetic maps from molecular dynamics simulation. *J. Chem. Theory Comput. 11*, 5002−5011.
(91) Noé, F., and Nuske, F. (2013) A variational approach to modeling slow processes in stochastic dynamical systems. *Multiscale Model. Simul. 11*, 635−655.
(92) Nüske, F., Keller, B., Pérez-Hernández, G., Mey, A. S., and Noé, F. (2014) Variational approach to molecular kinetics. *J. Chem. Theory Comput. 10*, 1739−1752.
(93) McGibbon, R. T., and Pande, V. S. (2015) Variational cross-validation of slow dynamical modes in molecular kinetics. *J. Chem. Phys. 142*, 03B621_621.
(94) Beauchamp, K. A., Bowman, G. R., Lane, T. J., Maibaum, L., Haque, I. S., and Pande, V. S. (2011) MSMBuilder2: modeling conformational dynamics at the picosecond to millisecond scale. *J. Chem. Theory Comput. 7*, 3412.
(95) Trendelkamp-Schroer, B., and Noé, F. (2013) Efficient Bayesian estimation of Markov model transition matrices with given stationary distribution. *J. Chem. Phys. 138*, 164113.
(96) Swope, W. C., Pitera, J. W., and Suits, F. (2004) Describing protein folding kinetics by molecular dynamics simulations. 1. Theory. *J. Phys. Chem. B 108*, 6571−6581.
(97) Röblitz, S., and Weber, M. (2013) Fuzzy spectral clustering by PCCA+: application to Markov state models and data classification. *Advances in Data Analysis and Classification 7*, 147−179.
(98) Singhal, N., and Pande, V. S. (2005) Error analysis and efficient sampling in Markovian state models for molecular dynamics. *J. Chem. Phys. 123*, 204909.
(99) Noé, F., Schütte, C., Vanden-Eijnden, E., Reich, L., and Weikl, T. R. (2009) Constructing the equilibrium ensemble of folding pathways from short off-equilibrium simulations. *Proc. Natl. Acad. Sci. U. S. A. 106*, 19011−19016.
(100) McGibbon, R. T., Beauchamp, K. A., Harrigan, M. P., Klein, C., Swails, J. M., Hernández, C. X., Schwantes, C. R., Wang, L.-P., Lane, T. J., and Pande, V. S. (2015) MDTraj: A Modern Open Library for the Analysis of Molecular Dynamics Trajectories. *Biophys. J. 109*, 1528−1532.
(101) Michino, M., Boateng, C. A., Donthamsetti, P., Yano, H., Bakare, O. M., Bonifazi, A., Ellenberger, M. P., Keck, T. M., Kumar, V., Zhu, C., Verma, R., Deschamps, J. R., Javitch, J. A., Newman, A. H., and Shi, L. (2017) Towards understanding the structural basis of partial agonism at the dopamine D3 receptor. *J. Med. Chem. 60*, 580.
(102) Stolzenberg, S., Khelashvili, G., and Weinstein, H. (2012) Structural Intermediates in a Model of the Substrate Translocation Path in the Bacterial Glutamate Transporter Homologue GltPh. *Biophys. J. 102*, 519a.
(103) Bochevarov, A. D., Harder, E., Hughes, T. F., Greenwood, J. R., Braden, D. A., Philipp, D. M., Rinaldo, D., Halls, M. D., Zhang, J., and Friesner, R. A. (2013) Jaguar: A high-performance quantum chemistry software program with strengths in life and materials sciences. *Int. J. Quantum Chem. 113*, 2110−2142.
(104) Brooks, B. R., Brooks, C. L., 3rd, Mackerell, A. D., Jr., Nilsson, L., Petrella, R. J., Roux, B., Won, Y., Archontis, G., Bartels, C., Boresch, S., Caflisch, A., Caves, L., Cui, Q., Dinner, A. R., Feig, M., Fischer, S., Gao, J., Hodoscek, M., Im, W., Kuczera, K., Lazaridis, T., Ma, J., Ovchinnikov, V., Paci, E., Pastor, R. W., Post, C. B., Pu, J. Z., Schaefer, M., Tidor, B., Venable, R. M., Woodcock, H. L., Wu, X., Yang, W., York, D. M., and Karplus, M. (2009) CHARMM: the biomolecular simulation program. *J. Comput. Chem. 30*, 1545−1614.
(105) Im, W., Lee, M. S., and Brooks, C. L. (2003) Generalized born model with a simple smoothing function. *J. Comput. Chem. 24*, 1691−1702.

DOI: 10.1021/acschemneuro.7b00094
ACS Chem. Neurosci. 2017, 8, 1735−1746